The Astrophysical Journal, 567:1077–1090, 2002 March 10

SPECTRA OF THE EXPANSION STAGE OF X-RAY BURSTS

Nickolai Shaposhnikov[1] and Lev Titarchuk[2,3]

Received 2001 September 21; accepted 2001 November 9

ABSTRACT

We present an analytical theory of thermonuclear X-ray burst atmosphere structure. Newtonian gravity and diffusion approximation are assumed. Hydrodynamic and thermodynamic profiles are obtained as a numerical solution of the Cauchy problem for the first-order ordinary differential equation. We further elaborate a combined approach to the radiative transfer problem that yields the spectrum of the expansion stage of X-ray bursts in an analytical form in which Comptonization and free-free absorption-emission processes are accounted for and $\tau \sim r^{-2}$ opacity dependence is assumed. A relaxation method on an energy opacity grid is used to simulate a radiative diffusion process in order to match the analytical form of the spectrum, which contains the free parameter, to the energy axis. Numerical and analytical results show high similarity. All spectra consist of a power-law soft component and a diluted blackbody hard tail. We derive simple approximation formulae usable for mass-radius determination by observational spectra fitting.

Subject headings: radiation mechanisms: nonthermal — stars: neutron — X-rays: binaries — X-rays: bursts

1. INTRODUCTION

First discovered by Grindlay & Heise (1975), strong X-ray bursts are believed to occur as the result of thermonuclear explosions in the bottom helium-reach layers of the atmosphere accumulated by a neutron star during the accretion process in a close binary system. Since then, dozens of burster-type X-ray sources were found. One of the distinctive feature of type I X-ray bursts is the sudden and abrupt ($\sim$1 s) luminosity increase (expansion stage) followed by exponential decay (contraction stage). Energy released in X-ray radiation during the first seconds greatly exceeds the Eddington limit for layers above the helium-burning zone that are no longer dynamically stable. Supercritically irradiated shells of atmosphere start to move outward, producing an expanding windlike envelope. The average lifetime of an X-ray burst is sufficient for a steady state regime of mass loss to be established when the local luminosity throughout most of the atmosphere is equal to or slightly greater than the Eddington limit.

During the last two decades the problem of determining properties of radiatively driven winds during X-ray bursts has been subjected to extensive theoretical and numerical studies. Various theories have been put forward, with gradually increasing levels of accuracy, of the problem description, but only a few approaches have addressed the case of a considerably expanded photosphere under the influence of near-Eddington luminosities (London, Taam, & Howard 1986; Ebisuzaki 1987; Lapidus 1991; Titarchuk 1994, hereafter T94). See Lewin, van Paradijs, & Taam (1993) for a detailed review of X-ray burst studies during the 1980s and the beginning of the 1990s.

Similarly to the problem of accretion flows, the notion of the existence of sonic points in continuous flows became a natural starting point in the analysis of wind flows from stellar objects. Ebisuzaki, Hanawa, & Sugimoto (1983, hereafter EHS) investigated the structure of the envelopes with steady state mass outflow and pointed out the higher Eddington luminosity in the inner shells due to the prevalent higher temperatures and correspondingly lower Compton-scattering opacities. They showed that the product of opacity and luminosity remains almost constant throughout the atmosphere, which is the key assumption of the model. The existence of windlike solutions for critically irradiated atmospheres was proved. T94 analytically studied spectral shapes of the expansion and contraction stages of bursts. He showed how EHS's approach to the hydrodynamic problem can be greatly simplified with the sonic point condition properly calculated and tied to conditions at the bottom of the envelope. Haberl & Titarchuk (1995) applied the T94 model to extract the neutron star mass-radius relations from the observed burst spectra in 4U 1820−30 and 4U 1705−44.

Nobili, Turolla, & Lapidus (1994, hereafter NTL) adopted a high-accuracy numerical approach to the problem of X-ray burster atmosphere structure based on the moment formalism (Thorne 1981; Nobili, Turolla, & Zamperi 1991). They integrated a self-consistent system of frequency-independent, relativistic, hydrodynamical, and radiative transfer equations over the whole atmosphere including the inner dense helium-burning shells. Three important characteristics of X-ray burst outflow were obtained in this work: the helium-burning zone temperature was maintained approximately at the level of 3×10^9 K, the temperature of the photosphere was shown to depart appreciably from the electron temperature and to stay constant at the outer shells, and the existence of the maximum and the minimum values of the mass-loss rate was found.

One of the goals of these studies was to provide the algorithm of determination of the compact object characteristics by analyzing observational data. With the advent of high spectral- and time-resolution observational instruments (such as *Chandra*, *Rossi X-Ray Timing Explorer* [*RXTE*], *Unconventional Stellar Aspect* [*USA*], and *XMM-Newton*),

[1] George Mason University, School for Computational Sciences and Center for Earth Observing and Space Research, Fairfax, VA 22030; nshaposh@scs.gmu.edu.

[2] George Mason University, Center for Earth Observing and Space Research, Fairfax, VA 22030; and US Naval Research Laboratory, Code 7620, Washington, DC 20375-5352; lev@xip.nrl.navy.mil.

[3] NASA Goddard Space Flight Center, Greenbelt, MD 20771; lev@lheapop.gsfc.nasa.gov.

the task of obtaining a suitable tool for fitting the energy spectra became extremely important. Despite numerous earlier studies of X-ray burst observations, recent developments have shown a growing interest of the astrophysical community in this area (Strohmayer & Brown 2002; Kuulkers et al. 2002a).

Obviously, the problem of radiative transfer in relativistically moving media is a very complicated one and, under rigorous consideration, it must be solved numerically. In this paper we develop an alternative approach that allows both numerical and analytical solutions and successfully accounts for all crucial physical processes involved. We show how this problem, under some appropriate approximations, yields the spectrum of radiation from spherically symmetric outflows in an analytical form. We concentrate on the case of extended atmospheres with inverse cubic power dependence of the number density on the radius, which is more appropriate for the expansion stage but can also be employed for description of the contraction as a sequence of models with decreasing mass-loss rate.

We represent a numerical approach to the problem that then provides the validation of our analytical description. We adopt the general approach formulated in EHS and developed in T94. The problem of determining profiles of thermodynamic variables of steady state radiatively driven outflow was solved in T94. The problem is reduced to the form of a first-order differential equation, which allows easy and precise numerical solutions. For completeness we present this method in § 2. Using atmospheric profiles obtained for different neutron star configurations, we solve the problem of radiative transfer by a relaxation method on an energy-opacity logarithmic grid. We perform temperature profile correction by applying temperature equations to the obtained spectral profiles. The basic formulae are given in § 3.1. Then, the analytical description of the problem is represented in detail. The analytic solution of the radiative transfer equation on the atmospheric profile $\tau \sim r^{-2}$ is presented in T94. Here, we review the solution by carrying out the integration without introducing any approximations. In § 4 we compare and match our analytical and numerical results to describe the behavior of the free parameter. We finalize our work by examining the properties of our analytic solution, combine it with the results of § 4, and construct the final formula for fitting the spectra in § 5. The discussion of our method along with some other important issues concerning the problem being solved are presented in § 6. Conclusions follow in § 7.

2. HYDRODYNAMICS

As we already mentioned, the calculation of X-ray burst spectra can be treated as a steady state problem. To justify this assumption one has to compare the characteristic times of phenomena considered. The timescale for the photosphere to collapse can be estimated as follows:

$$t_{\rm coll} = \int_{r_s}^{r_{\rm ph}} \frac{dr}{v_{\rm coll}} ,$$

where

$$v_{\rm coll} \approx \sqrt{\frac{2GM_{\rm ns}}{r}(1-l)} .$$

Here r_s denotes the sonic point radius, which is adopted as the outer boundary of the photosphere throughout this paper. The dimensionless luminosity is $l = L/L_{\rm Edd}$, where the Eddington luminosity is given by

$$L_{\rm Edd} = \frac{4\pi c G M_{\rm ns}}{\kappa} . \quad (1)$$

The opacity κ is expressed by the Compton scattering opacity with a Klein-Nishina correction by (Paczyński 1983)

$$\kappa = \frac{\kappa_0}{(1+\alpha T)} , \quad (2)$$

$\kappa_0 = 0.2(2 - Y_{\rm He})$ cm^2 g^{-1}, with $Y_{\rm He}$ being the helium abundance, and $\alpha = 2.2 \times 10^{-9}$ K^{-1}. It is exactly this temperature dependence of the opacity that is responsible for the excessive radiation flux, which appears to be super-Eddington to the outer, less hot layers of the atmosphere. In the framework of strong X-ray bursts the following condition are usually satisfied: $r_s \gtrsim 10^3$ km $\gg r_{\rm ph}$, $l \sim 0.99$. Putting $m = M_{\rm ns}/M_\odot \sim 1$ results in a time of collapse of the order of several seconds, the observed time that a type I X-ray burst usually lasts. For evaluation of the time for photons to diffuse through the photosphere, we note that the number of scattering events is $N \approx \tau_{\rm ph}^2$ (see, for example, Rybicki & Lightman 1979), where $\tau_{\rm ph}$ is the total opacity of the photosphere, which is $\sim$10. The time for a photon to escape is

$$t_{\rm esc} \sim \frac{\tau_{\rm ph}^2}{\sigma_{\rm T} n_e c} \sim \frac{r_{\rm ph}}{c} \tau_{\rm ph} \sim 0.1 \text{ s} .$$

This indicates that the hydrodynamic structure develops at least 10 times slower than the photon diffusing time through the photosphere. Although these timescales can become comparable in cases of greatly extended atmospheres, generally a steady state approximation is acceptable.

2.1. *Basic Equations for Radiatively Driven Outflow*

The problem of mass loss as a result of radiatively driven wind was formulated by EHS. For the convenience of the reader we summarize all equations important for the derivations in the following sections and refer the reader to EHS for details. The system of equations describing steady state outflow in spherical symmetry consists of a well-known Euler (radial momentum conservation) equation:

$$v\frac{dv}{dr} + \frac{GM}{r^2} + \frac{1}{\rho}\frac{dP}{dr} = 0 , \quad (3)$$

the mass-conservation law

$$\frac{d}{dr}(4\pi r^2 \rho v) = 0 , \quad (4)$$

the averaged radiation transport equation in the diffusion approximation

$$\kappa L_r = -\frac{16\pi a c r^2 T^3}{3\rho}\frac{dT}{dr} , \quad (5)$$

and the entropy equation

$$vT\frac{ds}{dr} + \frac{1}{4\pi r^2 \rho}\frac{dL_r}{dr} = 0 , \quad (6)$$

where P, ρ, T, s, and L_r are, respectively, the pressure, the density, the temperature, the specific entropy, and the diffusive energy flux flowing through a shell at r.

The outflowing gas is taken to be ideal. The dimensionless coordinate y, which is the ratio of the radiation pressure P_r to the gas pressure P_g, is introduced by

$$y = \frac{P_r}{P_g} = \frac{\mu m_p}{k} \frac{aT^3/3}{\rho} , \tag{7}$$

where $\mu = 4/(8 - 5Y_{\rm He})$ and m_p are the mean molecular weight and the proton mass, respectively. Then, the other thermodynamic quantities are expressed in terms of y and T as

$$P = P_r + P_g = \left(1 + \frac{1}{y}\right) \frac{aT^4}{3} , \tag{8}$$

$$\rho = \frac{a\mu m_p}{3k} \frac{T^3}{y} , \tag{9}$$

$$s = \left(\frac{k}{\mu m_p}\right)\left[4y + \ln y - \left(\frac{3}{2}\right) \ln T\right] , \tag{10}$$

$$h = \frac{k}{\mu m_p} \left(4y + \frac{5}{2}\right) T , \tag{11}$$

where h is the specific enthalpy.

The integrals of equations (4) and (3) give the mass flow and energy flux, correspondingly:

$$4\pi r^2 \rho v = \Phi , \tag{12}$$

$$\left(\frac{v^2}{2} - \frac{GM}{r} + h\right)\Phi + L_r = \Psi . \tag{13}$$

To make two more integrations, which cannot be performed analytically, the constancy of κL_r, which stands for the integral of equation (5), over the relevant layers is assumed. In EHS, this assumption is confirmed numerically. We can also justify it by the following consideration. At the near-Eddington regime, the radiation pressure $aT^4/3$ is much greater than the pressure of gas almost everywhere except for the innermost layers adjacent to the helium-burning zone. Neglecting the gas pressure in equation (3) and multiplying it by $-r^2$, we get

$$\frac{\kappa L_r}{4\pi c} = GM + r^2 v \frac{dv}{dr} . \tag{14}$$

Here, we moved the first two terms of equation (3) to the right-hand side and used equation (5) to express the third term by κL_r. For the inner and intermediate layers of the atmosphere, the last term in equation (14) is negligible, and the equation reduces to $\kappa L_r = \kappa_0 L_0$. This term can become considerably large for the outermost layers where L_r must exceed $L_{\rm Edd}$. This is also in agreement with observations of X-ray bursts from which super-Eddington luminosities are inferred. For the sake of analytical consideration, we consider κL_r to be constant throughout the whole atmosphere, and the third integral is

$$\kappa L_r = \kappa_0 L_0 = {\rm const} . \tag{15}$$

Replacing L_r of equation (6) with equation (15), the fourth integral is obtained as

$$\Phi s + \alpha L_0 \ln T = \Xi = {\rm const} . \tag{16}$$

Boundary conditions need to be imposed at the bottom and outer boundaries to determine the four integration constants Φ, Ψ, L_0, and Ξ and to obtain a specific solution.

At the bottom of the atmosphere close to the helium-burning zone there should be a point where the gas and radiation pressures are equal. As another important numerical result, EHS showed that near the neutron star surface the temperature and radius profiles level off with respect to y, so there is always a point where

$$r = r_b , \quad T = T_b , \quad y = 1 , \tag{17}$$

and r_b is well approximated by the radius of the neutron star $R_{\rm ns}$. However, T_b cannot be considered as a real temperature of the helium-burning shell at the bottom of the star surface because thermonuclear processes are not included in the model. The rigorous account of helium burning in NTL shows that the temperatures of burning shells vary in a small range of values.

To obtain the outer boundary condition, the concept of the sonic point is used. For the solution to be steady state and to have finite terminal velocity, it should pass the sonic point, where

$$v_s^2 = \frac{GM_{\rm ns}}{2r_s} = \left(\frac{\partial P_s}{\partial \rho_s}\right)_\Xi = \left(\frac{k}{\mu m_p}\right) Y_s T_s , \tag{18}$$

$$Y_s = \frac{\lambda + 4(1 + y_s)(1 + 4y_s)}{\lambda + 3(1 + 4y_s)} , \tag{19}$$

where λ is a quantity related to the ratio of the energy flux to the mass flux (see eq. [22] below). In EHS this formula contains a typographical error. We give a proper derivation of this form for Y_s in Appendix C.

2.2. *Ordinary Differential Equation Solution of the Hydrodynamic Problem*

T94 has shown how the treatment of the hydrodynamic problem can be reduced to a Cauchy problem with the boundary condition determined at the sonic point. This treatment provides a high-accuracy method of obtaining the hydrodynamic solution. The crucial point is to relate the position of the sonic point with the values of the velocity and the thermodynamic quantities before solving the set of appropriate hydrodynamic equations. The profile of the expanded envelope is then obtained as a result of the integration of a single first-order ordinary differential equation (ODE) from the sonic point inward up to the neutron star surface. For completeness we present the details of this approach.

At the bottom of the atmosphere the potential energy per unit mass of the gas, GM/r, is significantly greater than the kinetic energy, $v^2/2$, and enthalpy. Therefore, by ignoring these terms in equation (13), we obtain the value of the mass flux:

$$\Phi = \frac{R_{\rm ns}}{GM_{\rm ns}} \alpha T_b L_{\rm Edd}^0 . \tag{20}$$

The inner boundary condition (17), the integral (16), and equation (10) for entropy can be used to find the temperature distribution with respect to y:

$$T = T_b y^{-1/\lambda} \exp\left[-\frac{4(y-1)}{\lambda}\right] , \tag{21}$$

$$\lambda = \frac{\alpha \mu m_p}{k\Phi} L_0 - \frac{3}{2} . \quad (22)$$

The condition at the sonic point (18) allows us to find the constant Ψ:

$$\Psi = h_s \Phi + L_r(r_s) - \frac{3}{4} \frac{GM}{r_s} \Phi . \quad (23)$$

Combining the mass- and energy-conservation laws (12) and (13), the specific enthalpy and density equations (9) and (11), and eliminating the radial coordinate r between equations (12) and (13) yields the following dependence of the velocity derivative v' with respect to y:

$$v'_y(y, v) = v\left[\left(1 + 3\,\frac{1+4y}{\lambda}\right)\frac{1}{y} - 75.2\,\frac{rT(8 - 5Y_{\rm He})(1+4y)(1+\alpha T)}{\lambda r_{b,6}\, T_{b,9}(\Psi/\Phi - v^2/2 - h + GM_{\rm ns}/r)}\right] . \quad (24)$$

The derivation of equation (24) is given in Appendix D.

By imposing boundary conditions at the bottom of the extended envelope (at the neutron star surface) and at the sonic point, we can determine the four integration constants necessary to obtain a specific solution. One can note the obvious fact that the bottom of the envelope cannot serve as a starting point of integration of equation (24) as long as $v_b = 0$, which introduces uncertainty. Fortunately, we can calculate parameters at the sonic point in the framework of our problem description by solving a nonlinear algebraic equation that involves only y_s, the ratio of the radiation pressure P_r to the gas pressure P_g at that point. Substitution of the radial coordinate r_s and velocity v_s from the definition of the sonic point position (18), and the sonic point density ρ_s from equation (9), we find

$$r_s = \frac{GM_{\rm ns}\,\mu m_p}{2kY_s T_s} , \quad v_s = \left(\frac{k}{\mu m_p} Y_s T_s\right)^{1/2} ,$$

$$\rho_s = \frac{a\mu m_p}{3k} \frac{T_s^3}{y_s} ,$$

and the expression for the temperature given in equation (21) into the mass-conservation law (12), after some algebra, give an equation for the value of y_s:

$$y_s = \frac{\lambda}{4} \ln\left\{\left[\frac{(2 - Y_{\rm He})m^2}{r_{b,6}\, T_{b,9}}\right]^{2/3} \times \frac{T_b}{0.149(8 - 5Y_{\rm He})^{5/3} Y_s\, y_s^{1/\lambda + 2/3}}\right\} + 1 . \quad (25)$$

Here $r_{b,6}$ and $T_{b,9}$ are the neutron star surface radius and temperature in units of 10^6 cm and 10^9 K, respectively. Since Y_s is expressed in terms of y_s (eq. [19]), equation (25) can be solved to determine the value of y_s. Knowledge of y_s can then, by substitution in equation (21), yield the value of the temperature at the sonic point T_s and then v_s from equation (18). It is now possible to relate v_s to T_s, T_b, r_s, and r_b, thus obtaining the analytical expression for the various dynamical quantities at the sonic point in terms of the values of the parameters associated with the boundary conditions. To obtain the solution of the hydrodynamical problem for a particular set of input parameters, we use the standard Matlab/Octave package function *minimizators* and ODE solvers.

3. RADIATIVE TRANSFER PROBLEM

The radiation field of X-ray burst atmosphere may be described by the diffusion equation, written in spherical geometry, with the Kompaneets's energy operator (see T94):

$$\frac{1}{3}\left(\frac{\partial^2 J_\nu}{\partial \tau^2} - \frac{2}{r\alpha_{\rm T}} \frac{\partial J_\nu}{\partial \tau}\right) = \frac{\alpha_{\rm ff}}{\alpha_{\rm T}} (J_\nu - B_\nu) - \frac{kT_e}{m_e c^2} x_0 \frac{\partial}{\partial x_0}\left(x_0 \frac{\partial J_\nu}{\partial x_0} - 3J_\nu + \frac{T_0}{T} J_\nu\right) , \quad (26)$$

where $x_0 = h\nu/kT_0$ is a dimensionless frequency, T_0 being the effective temperature; and $\alpha_{\rm ff}$ and $\alpha_{\rm T} = \sigma_{\rm T} n_e$ are the coefficients of free-free absorption and Thompson scattering, respectively, whose ratio is given by (Rybicki & Lightman 1979)

$$\frac{\alpha_{\rm ff}}{\alpha_{\rm T}} = 1.23\rho g_{14}^{7/8}\left(1 - \frac{Y_{\rm He}}{2}\right)^{7/8} \Psi(x_0)\left(\frac{T_0}{T}\right)^{1/2} \quad (27)$$

with

$$\Psi(x_0) = \frac{\tilde{g}(x_0\, T_0/T)}{x_0^3} (1 - e^{-x_0 T_0/T}) .$$

Here $\tilde{g}(x)$ is the Gaunt factor (Greene 1959)

$$\tilde{g}(x) = \frac{\sqrt{3}}{\pi} e^{x/2} K_0\left(\frac{x}{2}\right) ,$$

$K_0(x)$ is the Macdonald function, and g_{14} denotes the free-fall acceleration onto the neutron star surface in units of 10^{14} cm s^{-1}.

We combine equation (26) with the outer boundary condition of zero energy inflow

$$\left.\left(\frac{\partial J_\nu}{\partial \tau} - \frac{3}{2} J_\nu\right)\right|_{\tau=0} = 0 \quad (28)$$

and the condition of equilibrium blackbody spectrum at the bottom of the photosphere, which is represented in a dimensionless form as

$$B_\nu = \frac{x_0^3}{\exp(x_0\, T_0/T) - 1} . \quad (29)$$

We will make use of the temperature equation, which is obtained by integration of equation (26) over frequency. The opacity operator vanishes as a result of the total flux conservation with respect to optical depth, leaving us with

$$\frac{kT_e}{mc^2}\left(4\int_0^\infty J_\nu\, dx_0 - \frac{T_0}{T}\int_0^\infty x_0 J_\nu\, dx_0\right) = 1.23\rho g_{14}^{7/8}\left(1 - \frac{Y_{\rm He}}{2}\right)^{7/8}\left(\frac{T_0}{T}\right)^{1/2} \times \left[\int_0^\infty J_\nu \Psi(x_0) dx_0 - \frac{2\sqrt{3}}{\pi}\frac{T}{T_0}\right] . \quad (30)$$

In the condition of the extended photosphere of X-ray bursts, the density is usually very low and the left-hand side of the last equation can be neglected, reducing the last equation to the formula for temperature:

$$\frac{T}{T_0} = \frac{1}{4}\left(\int_0^\infty x_0 J_\nu\, dx_0 \Big/ \int_0^\infty J_\nu\, dx_0\right) . \quad (31)$$

We will use the last relation to produce a corrected temperature profile for the photosphere where it departs significantly from that given by the hydrodynamic solution.

3.1. *Analytic Description of Radiative Diffusion*

Hydrodynamic profiles calculated in § 2 show that during the expansion stage in the vicinity of the sonic point $v \sim v_s(r/r_s)$. Considering this relation to be true throughout the entire envelope, according to the mass-conservation law, we can write

$$n_e = \frac{\rho}{m_p}\left(1 - \frac{Y_{\rm He}}{2}\right) = \frac{\Phi}{4\pi m_p v r^2} = \frac{GM\Phi}{8\pi v_s^3 m_p}\left(1 - \frac{Y_{\rm He}}{2}\right) r^{-3} , \quad (32)$$

where Φ is the mass-loss rate and v_s is the velocity of gas at the sonic point. In this case opacity can be expressed as

$$\tau = C \int_r^\infty \frac{\sigma_{\rm T}}{r^3}\, dr = \frac{C\sigma_{\rm T}}{2r^2} . \quad (33)$$

Noting that in this case

$$\tau = \frac{r\alpha_{\rm T}}{2} , \quad (34)$$

we can rewrite the radiation transfer equation in the form

$$\frac{\partial}{\partial \tau}\frac{1}{\tau}\frac{\partial J_\nu}{\partial \tau} = \frac{3}{\tau}\frac{\alpha_{\rm ff}}{\alpha_{\rm T}}(J_\nu - B_\nu) - \frac{3kT_e}{m_e c^2 \tau} L_\nu(J_\nu) . \quad (35)$$

The boundary conditions are given by

$$J_\nu |_{\tau = \tau_{\rm th}} = B_\nu(\tau_{\rm th}) \quad (36)$$

at the inner boundary of the photosphere and

$$H = \frac{4\pi}{3}\int_0^\infty \frac{\partial J_\nu}{\partial \tau}\, d\nu |_{\tau=0} = \frac{L}{4\pi R_s^2} \quad (37)$$

at the sonic surface. The ratio $\alpha_{\rm ff}/\alpha_{\rm T}$ can be written in the form

$$\frac{\alpha_{\rm ff}}{\alpha_{\rm T}} = 1.23\left(1 - \frac{Y_{\rm He}}{2}\right)^{-5/8}\left(\frac{2m_p}{\sigma_{\rm T}}\right)^{3/2}\left(\frac{8\pi v_s^3}{GM\Phi}\right)^{1/2} \times g_{14}^{-7/8}\frac{\tilde{g}(x)(1 - e^{-x})}{x^3}\left(\frac{T_0}{T}\right)^{7/2}\tau^{3/2} = D\Psi(x)\tau^{3/2} , \quad (38)$$

where $x = h\nu/kT_e$ and $\Psi(x) = \tilde{g}(x)(1 - e^{-x})/x^3$.

Stated in this way, the problem of radiative transfer allows an analytical approach. The solution of the radiative transfer equation (35) is

$$J(t, x) = B_\nu \frac{t^{8/7}}{2^{4/7}\Gamma(11/7)}\left[\frac{\Gamma(3/7)}{2^{4/7}} + \frac{8}{7} t_{\rm th}^{-4/7} K_{4/7}(t_{\rm th})\right] , \quad (39)$$

where K_p is the modified Bessel function of the first kind, and

$$t = \tfrac{4}{7}\sqrt{3D\Psi(x)}\tau^{7/4} . \quad (40)$$

Details of the derivation of this formula are given in Appendix A.

3.2. *Evaluation of* $\tau_{\rm th}$ *and* T_c

The next step is to find the color temperature and to determine the thermalization depth $\tau_{\rm th}$ where the boundary condition (36) is valid. For saturated Comptonization, the occupation number behaves in accordance with the Bose-Einstein photon distribution $n = (e^{\mu + x} - 1)^{-1}$, which might be described as a diluted blackbody spectrum or a diluted Wien distribution.

At first we evaluate the color temperature assuming a blackbody spectral shape. We look for the solution of the form

$$n(\tau, x) = \frac{R(\tau)}{e^x - 1} . \quad (41)$$

The solution, which is described in detail in Appendix B, gives for $R(\tau)$

$$R(\tau) = 1 - \frac{2^{3/7}}{\Gamma(4/7)}\frac{\tau}{\tau_{\rm th}} K_{4/7}\left[\left(\frac{\tau}{\tau_{\rm th}}\right)^{7/4}\right] . \quad (42)$$

As long as $R(\tau) = 1$ for $\tau > \tau_{\rm th}$, there is radiation equilibrium for optical depths deeper than the photospheric envelope. The temperature equation in the zone $0 < \tau < \tau_{\rm th}$ reads

$$\left(\frac{T}{T_0}\right)^4 = \frac{2H_0}{R^2}\left(\frac{3}{2\tau_R}\int_0^\tau \tau d\tau + 2\right)\Big/\frac{\pi^4}{15}R(\tau)$$

where $H_0 = (4\pi R_{\rm ns}^2 \pi^5/15)/16\pi^2$ and τ_R (<1) is the optical depth coordinate at the outer boundary of the expanded atmosphere, $r = R$ (see eq. [35]). This equation can be rewritten as follows:

$$\left(\frac{T}{T_0}\right)^4 = \frac{3\tau^2/4 + 2\tau_R}{2\tau_{\rm ns} R(\tau)} . \quad (43)$$

Neglecting τ_R with respect to τ and making use of Taylor expansion (B6) of $R(\tau)$ we get a constant value of the temperature

$$\left(\frac{T}{T_0}\right)^4 = \frac{3}{8}\frac{2^{8/7}\Gamma(11/7)}{\Gamma(3/7)}\frac{\tau_{\rm th}^2}{\tau_{\rm ns}} = 0.356\frac{\tau_{\rm th}^2}{\tau_{\rm ns}} . \quad (44)$$

Using the notation (see T94 for definition of x_*)

$$p = 2\tilde{g}(x_*) \approx \ln\left(\frac{2.35}{x_*}\right) , \quad (45)$$

formula (38) becomes

$$D = D_0\left(\frac{T_0}{T}\right)^{7/2} , \quad (46)$$

where

$$D_0 = 1.23\left(1 - \frac{Y_{\rm He}}{2}\right)^{-5/8}\left(\frac{2m_p}{\sigma_{\rm T}}\right)^{3/2}\left(\frac{8\pi v_s^3}{GM\Phi}\right)^{1/2} g_{14}^{-7/8} ,$$

while we can write for $\tau_{\rm th}$

$$\tau_{\rm th} = \left(\frac{4}{7}\sqrt{\tilde{D}}\right)^{-4/7} = \left(\frac{6}{49}p^2 D\right)^{-2/7} = \frac{T}{T_0}\left(\frac{6}{49}p^2\right)^{-2/7} D_0^{-2/7} . \quad (47)$$

Substituting it into equation (44), we get for T/T_0

$$\frac{T}{T_0} = 0.596\left(\frac{6}{49}p^2\right)^{-2/7}\frac{D_0^{-2/7}}{\tau_{\rm ns}^{1/2}} . \quad (48)$$

Assuming the same electron number density as in equation (32), we then express opacity at the neutron star surface $\tau_{\rm ns}$ in the form

$$\tau_{\rm ns} = \left(1 - \frac{Y_{\rm He}}{2}\right)\left(\frac{\sigma_{\rm T}}{2m_p}\right)\left(\frac{GM\Phi}{8\pi v_s^3 R_{\rm ns}^2}\right) . \tag{49}$$

If we use the dependence of input parameters g_{14} and Φ on m, $r_{b,6}$, $T_{b,9}$ and $Y_{\rm He}$, the next useful equations for the color ratio T/T_0, color temperature kT, and thermalization depth $\tau_{\rm th}$ are found:

$$\frac{T}{T_0} = \frac{0.191(2 - Y_{\rm He})^{1/28} r_{b,6}^{1/7} v_{s,8}^{15/14}}{m^{3/28} T_{b,9}^{5/14} p^{4/7}} , \tag{50}$$

$$kT = 0.4 m^{1/7} r_{b,6}^{-5/14} T_{b,9}^{-5/14} v_{s,8}^{15/14} \times (2 - Y_{\rm He})^{-3/14} p^{-4/7} {\rm keV} , \tag{51}$$

$$\tau_{\rm th} = 90.5 m^{2/7} r_{b,6}^{-3/14} T_{b,9}^{-3/14} v_{s,8}^{9/14} \times (2 - Y_{\rm He})^{1/14} p^{-8/7} . \tag{52}$$

Here $v_{s,8}$ is the sonic point velocity in units of 10^8 cm s^{-1}. These relations present the final results of our analytical approach. There is still a lack of completeness due to the presence of p and v_s in the left-hand sides of this system of equations. The parameter p and the sonic point velocity are not independent parameters of the problem, but at this point they cannot be inferred from further analytical consideration. Fortunately, these quantities can be quite well approximated by a power dependence from m, $r_{b,6}$, $T_{b,9}$, and $(2 - Y_{\rm He})$, which is done in the next section.

4. NUMERICAL RESULTS AND COMPARISON WITH AN ANALYTICAL DESCRIPTION OF THE RADIATIVE TRANSFER PROBLEM

To confirm the validity of our analytical approach and to examine the behavior of p and v_s in dependence of different input parameters of the problem, we perform numerical modeling of the steady state radiative transfer process. The whole procedure consists of three steps.

First, for a particular model of neutron star, i.e., for a given mass and radius, we obtain a set of model atmospheres for a chosen set of bottom temperatures. These solutions provide us with runs of thermodynamical and hydrodynamical profiles, sonic point characteristics, masses of the extended envelopes, and their loss rates. Second, we solve the radiative transfer equation (26) on each model atmosphere obtained with the relaxation method (e.g., Press et al. 1992) on an energy-opacity grid using logarithmic scale on both dimensions. The energy range includes 500 grid points. The number of grid points in opacity varies between 100 and 300. The opacity domain includes the range $\tau_s < \tau < \tau_{\rm max}$, where τ_s is the opacity at the sonic point and $\tau_{\rm max}$ was taken large enough to meet the inequality $\tau_{\rm max} > \tau_{\rm th}$ safely. We use the mixed outer boundary condition (28). The spectrum at the inner bottom of the photosphere is taken as a pure blackbody B_ν. Numerical calculations of the frequency-dependent radiation field consist of two runs of our relaxation code. The first run is performed on a temperature continuum obtained from the hydrodynamical solution (see § 2.2). We then calculate a spectral temperature profile using formula (31), which exhibits a quite expected behavior. At some region this corrected profile departs from the initial temperature profile and levels off at some constant value in absolute agreement with the analytic result of § 3.2. It is also in qualitative agreement with the NTL self-consistent calculation of the radiation-driven wind structure of an X-ray burster. A second run is performed on the corrected profile to get a more reliable spectrum shape. At the final step we compare analytical and numerical solutions. The sonic point provides a natural position to match numerical and analytical solutions. Combining the sonic point parameters, calculated through the solution of equation (25) and using relation (34), we get for the opacity at the sonic point

$$\tau_s = \frac{\sigma_{\rm T}}{2m_p} r_s \rho_s \left(1 - \frac{Y_{\rm He}}{2}\right) . \tag{53}$$

We calculate and plot fluxes given by both methods at the sonic point. A particular value of parameter p for the analytic model is obtained by matching the value of kT and the corrected level of a numerically achieved value of photospheric temperature.

We obtained results for approximately 150 different sets of values T_b, $R_{\rm ns}$, $M_{\rm ns}$, and $Y_{\rm He}$. Examples of numerical calculations of spectra for different neutron star models and fitting them with analytical shapes are presented in Figures 1 and 2. Analytical and numerical shapes match quite well in the wide range of neutron star surface temperatures, and both show two distinctive features of outgoing spectrum of expansion stage: a diluted blackbody-like high-frequency component and power-law soft excess at the lower part. Dependence of the sonic point opacity presented by equation (53) describes correctly the dilution process, indicating that the assumption of atmosphere structure adopted in the analytical model is correct.

Tables 1 and 2, which summarize results for two different neutron star models, are given in order to compare our results with more rigorous calculations (NTL). Taking mass-loss rate as an input parameter, NTL obtained profiles of different quantities throughout the whole atmosphere. They argued that the temperature of the burning shell is maintained around 3×10^9 K for all models. The temperature of photons departs appreciably from the temperature of ambient matter above photospheric radius and stays practically constant, indicating that radiation becomes essentially decoupled from expanded media. We change the bottom temperature in a wide range of values and infer the mass-loss rate, the mass of envelope, etc.

Our results are in qualitative agreement with NTL. The crucial physical parameters that define the main spectral signatures are the photospheric radius $r_{\rm ph}$ and its temperature kT. Runs of the atmospheric profiles obtained by both approaches are quite similar, although $T_{\rm ph}$ in the results of NTL is usually 15%–25% greater than in our models. This difference is explainable. We match isothermal levels given by numerical and analytical calculations and define the obtained value as a photospheric temperature. This is the lowest estimation, because the temperature profile starts to grow before the bottom of the photosphere is reached. NTL define $T_{\rm ph}$ as a matter temperature at $r_{\rm ph}$. A temperature level calculated at the thermalization depth $\tau_{\rm th}$ should compensate the considered difference. The difference in density profiles, which can achieve a factor of 2, will affect the spectrum only in the soft part ($\leq$0.2 keV) where the normalization of the power-law component can be changed. This fact does not diminish the validity of our results. The soft component of the spectrum can be represented as an

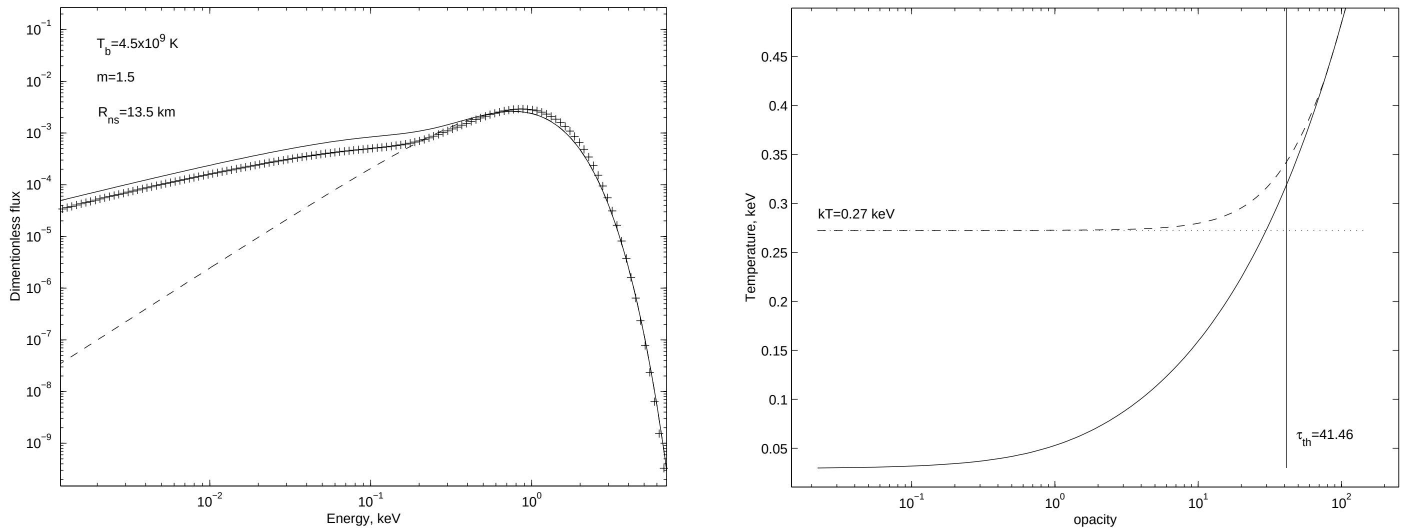

FIG. 1.—Examples of spectra (*left*) and temperature profiles (*right*) obtained for model with $m = 1.5$, $R_{\rm ns} = 13.5$ km, $Y_{\rm He} = 1$. On the left, the solid line represents the analytical solution, the dashed line indicates the diluted blackbody level, and the plus signs are the results of a relaxation method simulation. On the right, the solid line is the temperature profile obtained from the initial hydrodynamical solution, the dashed line is the corrected profile (see text), and the dotted line is the analytically calculated color temperature level.

independent fitting shape with a normalization included as an additional fitting parameter. This matter is not crucial at the moment because of the restricted spectral capabilities of current X-ray observing facilities. One can also notice a quick decrease of the envelope mass and point out a wide variation of T_b. This discrepancy can be explained by differences in model formulations. Specifically, NTL included helium-burning shells in the model and put the inner boundary condition on the "real" neutron star surface, while our model stops where radiation and gas pressures are equal ($y = 1$), which is close to but still outside of the helium-burning shell. In our approach, part of the bottom of the atmosphere is left out. In fact, the lower the mass-loss rate, the greater the portion of mass missing beyond the point where $y = 1$. This is clearly seen from the tables. The temperature at the bottom can be considered as an "effective" instead of the real temperature of the helium-burning zone.

As we have already pointed out, one needs to know the dependencies of v_s and p on input parameters to complete the analytical description and thus to employ these results to the fitting of observational X-ray spectra. Analysis of v_s and p runs show that log v_s and log p are linear functions of log T_b, log $R_{\rm ns}$, log $M_{\rm ns}$, and log $(2 - Y_{\rm He})$. We combine all experiments and fit $v_{s,\,8}$ and p with a model const $\times\, T^{\alpha}_{b,\,9}\, r^{\beta}_{b,\,6}\, m^{\gamma}(2 - Y_{\rm He})^{\eta}$ by the least-squares method to get

$$p = 7.69 T_{b,\,9}^{-0.84} r_{b,\,6}^{-0.89} m^{0.69} (2 - Y_{\rm He})^{-0.22}\,, \qquad (54)$$

$$v_{s,\,8} = 5.46 T_{b,\,9}^{-0.71} r_{b,\,6}^{-0.87} m^{0.63} (2 - Y_{\rm He})^{-0.22}\,, \qquad (55)$$

with maximum errors of parameters less than 1%. The ranges of parameters included in fitting are 0.3–7.0 for $T_{b,\,9}$, 0.6–2.0 for $r_{b,\,6}$, 0.8–2.7 for m, and 0.3–1.0 for $Y_{\rm He}$. These results can be used to substitute p and $v_{s,\,8}$ in equations (50), (51), and (52). Now we have a consistent system of equations that should yield the X-ray spectrum of the burster in the

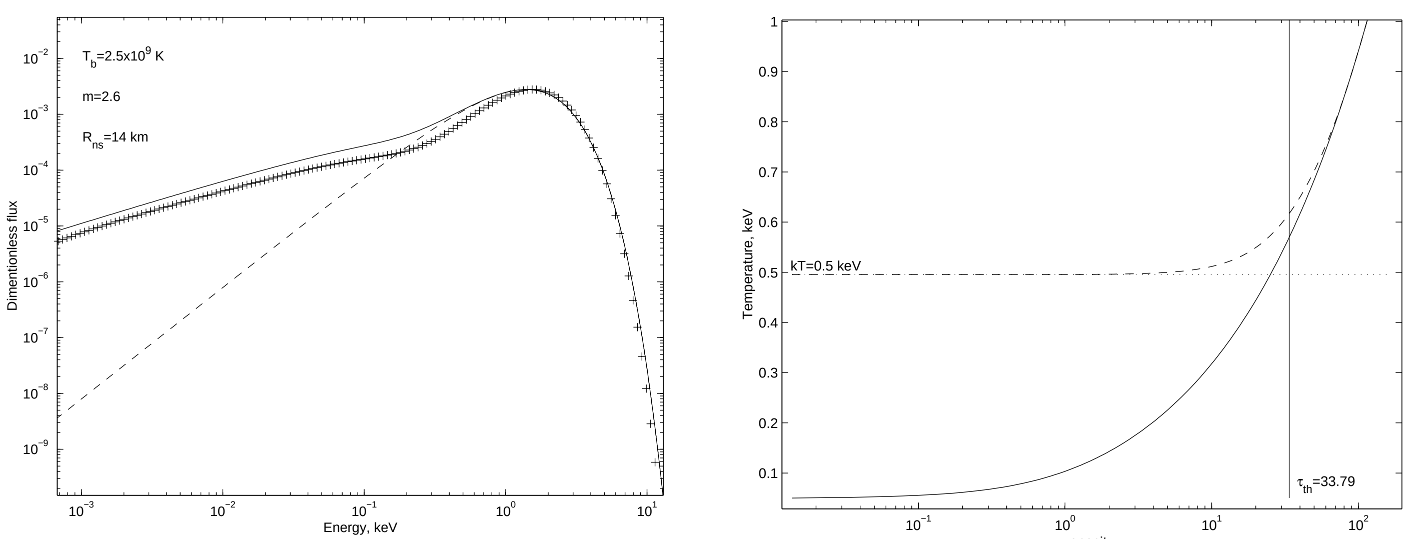

FIG. 2.—Same as Fig. 1, but for the model with $m = 2.6$, $R_{\rm ns} = 14$ km, $Y_{\rm He} = 1$

TABLE 1

PARAMETERS FOR MODEL $m = 1.5$, $R_{ns} = 13.5$ km, $Y_{He} = 1$

T_b (10^9 K)	kT (keV)	T/T_0	τ_{th}	p	Φ[a]	M_{env} (10^{22} g)	T_s (0.1 keV)	v_s (10^3 km s^{-1})	r_s (10^3 km)	r_{ph} (10^3 km)
7.0	0.197	0.099	45.1	1.56	93.9	173.3	0.21	1.31	57.9	4.16
6.5	0.208	0.105	44.7	1.64	87.2	128.9	0.22	1.39	51.6	3.71
6.0	0.221	0.111	44.1	1.75	80.5	93.6	0.24	1.48	45.6	3.28
5.5	0.236	0.118	43.3	1.87	73.8	66.1	0.25	1.58	39.9	2.88
5.0	0.252	0.127	42.4	2.02	67.1	45.1	0.27	1.70	34.5	2.50
4.5	0.272	0.137	41.5	2.20	60.4	29.6	0.29	1.84	29.4	2.14
4.0	0.295	0.148	40.3	2.42	53.7	18.5	0.32	2.01	24.6	1.80
3.5	0.324	0.163	39.0	2.71	46.9	10.9	0.35	2.22	20.1	1.48
3.0	0.359	0.180	37.4	3.09	40.2	5.86	0.39	2.50	16.0	1.19
2.5	0.406	0.204	35.6	3.60	33.5	2.83	0.44	2.85	12.2	0.92
2.0	0.470	0.236	33.4	4.34	26.8	1.16	0.51	3.36	8.83	0.67
1.75......	0.510	0.257	32.2	4.85	23.5	0.68	0.55	3.69	7.29	0.56
1.5	0.565	0.284	30.8	5.53	20.1	0.37	0.61	4.12	5.86	0.45
1.25......	0.634	0.318	29.2	6.44	16.8	0.179	0.68	4.69	4.53	0.36
1.1	0.686	0.344	28.0	7.18	14.8	0.108	0.74	5.12	3.80	0.30
1.0	0.727	0.365	27.2	7.78	13.4	0.074	0.78	5.47	3.33	0.27
0.9	0.775	0.389	26.3	8.51	12.1	0.049	0.84	5.87	2.89	0.23
0.8	0.831	0.417	25.3	9.40	10.7	0.031	0.90	6.36	2.46	0.20
0.7	0.898	0.451	24.3	10.5	9.4	0.018	0.97	6.95	2.06	0.17
0.6	0.981	0.492	23.0	12.0	8.0	0.010	1.06	7.69	1.68	0.14
0.5	1.086	0.545	21.6	14.0	6.7	0.005	1.17	8.65	1.33	0.11
0.4	1.224	0.614	19.9	17.0	5.4	0.002	1.32	9.95	1.01	0.09
0.3	1.417	0.711	17.8	21.9	4.0	0.001	1.53	11.8	0.71	0.07

[a] Φ is in units of the critical mass-loss rate, i.e., divided by L_{Edd}/c^2.

form of a function of only input physical parameters, i.e., neutron star mass, radius, surface temperature, and elemental abundance.

5. FINAL FORM OF THE PROFILE FOR SPECTRAL FITTING

The fact that spectra obtained are blackbody-like almost everywhere except for small values of energies allows us to proceed with simplification of the formula (39). First we note that as a result of equation (47) and the smallness of x,

$$t_{th} = \frac{4}{7}\sqrt{3\Psi(x)D}\tau_{th}^{7/4} = 2\,\frac{\sqrt{2\Psi(x)}}{p} \simeq 2\,\frac{\sqrt{\ln(2.35/x)}}{px} \quad (56)$$

for the soft part of the spectrum. Here $x = h\nu/kT$, $\Psi(x)$, and D are defined in formulae (27) and (46), correspondingly.

TABLE 2

PARAMETERS FOR MODEL $m = 2.6$, $R_{ns} = 14.0$ km, $Y_{He} = 1$

T_b (10^9 K)	kT (keV)	T/T_0	τ_{th}	p	Φ	M_{env} (10^{22} g)	T_s (0.1 keV)	v_s (10^3 km s^{-1})	r_s (10^3 km)	r_{ph} 10^3 km)
7.0	0.248	0.110	45.1	2.12	56.2	115.8	0.242	1.80	53.4	3.53
6.5	0.261	0.116	44.5	2.24	52.2	86.1	0.256	1.90	47.7	3.15
6.0	0.277	0.123	43.6	2.40	48.2	62.6	0.271	2.02	42.2	2.80
5.5	0.294	0.131	42.6	2.58	44.1	44.2	0.288	2.16	36.9	2.46
5.0	0.313	0.139	41.5	2.80	40.1	30.2	0.308	2.32	31.9	2.15
4.5	0.337	0.150	40.3	3.07	36.1	19.8	0.331	2.52	27.2	1.84
4.0	0.364	0.162	39.0	3.40	32.1	12.4	0.359	2.75	22.8	1.56
3.5	0.398	0.177	37.4	3.82	28.1	7.27	0.394	3.04	18.7	1.29
3.0	0.440	0.196	35.7	4.36	24.1	3.93	0.437	3.41	14.9	1.04
2.5	0.495	0.220	33.8	5.12	20.1	1.90	0.494	3.89	11.4	0.81
2.0	0.570	0.254	31.5	6.21	16.1	0.78	0.572	4.58	8.24	0.59
1.75......	0.620	0.276	30.2	6.97	14.0	0.46	0.623	5.03	6.80	0.50
1.5	0.682	0.304	28.7	7.97	12.0	0.25	0.687	5.61	5.47	0.40
1.25......	0.763	0.339	27.0	9.33	10.0	0.121	0.770	6.38	4.24	0.32
1.1	0.824	0.366	25.9	10.4	8.83	0.073	0.833	6.96	3.56	0.27
1.0	0.872	0.388	25.1	11.3	8.03	0.050	0.883	7.43	3.12	0.24
0.9	0.928	0.413	24.2	12.4	7.22	0.033	0.940	7.98	2.71	0.21
0.8	0.993	0.442	23.3	13.7	6.42	0.021	1.008	8.63	2.31	0.18
0.7	1.072	0.477	22.2	15.4	5.62	0.012	1.089	9.43	1.94	0.15
0.6	1.169	0.520	21.0	17.6	4.82	0.007	1.188	10.4	1.59	0.13
0.5	1.292	0.575	19.7	20.6	4.01	0.003	1.313	11.7	1.26	0.10
0.4	1.455	0.647	18.1	24.9	3.21	0.001	1.479	13.5	0.95	0.08
0.3	1.682	0.749	16.2	32.0	2.41	0.0005	1.710	16.0	0.67	0.06

Because $t_{\rm th}$ is large for small values of x, we can use an approximation of the modified Bessel function of the second kind for large arguments:

$$K_p(x) \approx \sqrt{\frac{\pi}{2x}}\, e^{-x} ,$$

and rewrite equation (39) as follows:

$$\begin{aligned} J(\tau, x) &= B_\nu\left(\frac{\tau}{\tau_{\rm th}}\right)^2 \\ &\quad \times \left[\frac{\Gamma(3/7)}{\Gamma(11/7)}\, z^{8/7} + \frac{4}{7\Gamma(11/7)}\, z^{1/14} e^{-2z}\right] \\ &= B_\nu\left(\frac{\tau}{\tau_{\rm th}}\right)^2 (2.32 z^{8/7} + 0.64 z^{1/14} e^{-2z}) , \end{aligned} \quad (57)$$

where

$$z = \frac{\sqrt{\ln(2.35/x)}}{px} .$$

Here we rewrite the dilution factor in terms of opacity using relation (40). Clearly, the second term in the parentheses of formula (57) is significant only where z becomes small (x becomes large) and the spectrum shape "adjusts" to the blackbody component. In turn, the first term of equation (57) represents the power-law component of the lower part of the spectrum with the slope $\frac{6}{7}$, which can be shown by simple similarity (see also T94):

$$B_\nu z^{8/7} \sim \frac{x^2}{x^{8/7}} = x^{6/7} .$$

Another important advantage of this term is that it vanishes for large values of x. This fact gives us the opportunity to construct a convenient and accurate formula for observational spectra fitting. We drop the second term in equation (57) and adjust to the diluted blackbody shape by means of a quadratic power combination as follows:

$$J(\tau, x) = B_\nu\left(\frac{\tau}{\tau_{\rm th}}\right)^2 (1 + 5.34 z^{16/7})^{1/2} . \quad (58)$$

Comparison of the shapes given by formula (58) with the exact solution of equation (39) shows that they deviate from each other by less than 2%, which is more than acceptable in contemporary astrophysical observational data analysis. Using the explicit form of z and the form of the outgoing flux, equation (58) can be rewritten in the form

$$\begin{aligned} F_\nu &= \frac{4\pi}{3}\frac{dJ_\nu}{d\tau} \\ &= \frac{8\pi}{3} B_\nu \frac{\tau_s}{\tau_{\rm th}^2}\left\{1 + 5.34\left[\frac{\ln(2.35/x)}{p^2 x^2}\right]^{8/7}\right\}^{1/2} . \end{aligned} \quad (59)$$

Equation (53) yields a useful relationship for the dilution coefficient in the manner similar to equations (50), (51), and (52):

$$\frac{8\pi}{3}\frac{\tau_s}{\tau_{\rm th}^2} = \frac{5.07 \times 10^{-5} r_{b,6}^{10/7} T_{b,9}^{10/17} p^{16/7}}{m^{11/7} v_{s,8}^{2/7} (2 - Y_{\rm He})^{1/7}} . \quad (60)$$

Substituting the results of parameters fitting equations (54) and (55), we get

$$\frac{8\pi}{3}\frac{\tau_s}{\tau_{\rm th}^2} = 3.31 \times 10^{-3} r_{b,6}^{-0.36} T_{b,9}^{-0.29} m^{-0.17} (2 - Y_{\rm He})^{-0.58} . \quad (61)$$

Here, again, $r_{b,6}$, $T_{b,9}$, and m are the neutron star radius, surface temperature, and mass in units of 10^6 cm, 10^9 K, and $M_\odot$, respectively. Now we have provided our spectrum profile (59) with expressions for parameter p (54) and the dilution factor (61). These three formulae constitute the final analytical results of this paper.

6. DISCUSSION

The model and derivations presented above assume that plasma consists of fully ionized hydrogen and helium. In reality, this assumption can be too simplistic. For instance, in the case of the recently discovered superbursts (Serpens X-1, Cornelisse et al 2002b; KS 1731−260, Kuulkers et al. 2002b; 4U 1735–44, Cornelisse et al. 2002a; 4U 1820–30, Strohmayer & Brown 2002), a sufficient fraction of material should be represented by heavier elements. These long and powerful bursts are also considered to be caused by the nuclear runaway burning in the carbon "ocean" under the neutron star surface. In this section we discuss how our model can be adjusted for the study of this phenomenon. The approach as a whole does not change, but some formulae have to be modified in order to account for the different plasma composition.

First, we note that for plasma that consists of a single ionized element, we have for the mean molecular weight

$$\mu = \frac{A}{1 + Z} ,$$

and for the electron number density

$$n_e = \frac{\rho}{A m_p} Z ,$$

where A and Z are the atomic weight and the atomic number of the corresponding element, respectively. In the general case of heterogeneous elements, each represented by weight abundance Y_i, we write

$$\mu = \frac{1}{\sum Y_i(1 + Z_i)/A_i} , \quad (62)$$

$$n_e = \frac{\rho}{m_p} \sum \frac{Z_i}{A_i} Y_i . \quad (63)$$

In the hydrodynamic part of this study, these modifications will affect only the form of the terms and factors containing $Y_{\rm He}$. In the radiation-transfer section, the form of $\alpha_{\rm ff}/\alpha_{\rm T}$ will require more careful treatment. According to Rybicki & Lightman (1979), the free-free absorption coefficient is

$$\alpha_{\rm ff} = 3.7 \times 10^8 T^{-1/2} \overline{Z^2 n_i}\, n_e \nu^{-3} (1 - e^{-h\nu/kT}) \tilde{g}_{\rm ff} , \quad (64)$$

where

$$\overline{Z^2 n_i} = \sum Z_i^2 n_i = \frac{\rho}{m_p} \sum \frac{Z_i^2}{A} Y_i . \quad (65)$$

In the case of a hydrogen-helium plasma this factor is conveniently represented by just gas density, i.e.,

$$\overline{Z^2 n_i} = n_{\rm H} + 4n_{\rm He} = \frac{\rho}{m_p}(Y_{\rm H} + Y_{\rm He}) = \frac{\rho}{m_p},$$

which yields equation (27). In general, one should use expressions (64) and (65) to find the correct form of $\alpha_{\rm ff}/\alpha_{\rm T}$ relevant to the specific chemical composition.

To be more instructive we conduct such a modification for the case when the plasma has a substantial carbon fraction. Using equations (62), (63), and (65), we write for hydrogen-helium-carbon gas:

$$\mu = \frac{12}{24Y_{\rm H} + 9Y_{\rm He} + 7Y_{\rm C}} = \frac{4}{8 - 5Y_{\rm He} - 17Y_{\rm C}/3}, \quad (66)$$

$$n_e = \frac{\rho}{m_p}\left(1 - \frac{Y_{\rm He} + Y_{\rm C}}{2}\right), \quad (67)$$

and

$$\overline{Z^2 n_i} = \frac{\rho}{m_p}(Y_{\rm H} + Y_{\rm He} + 3Y_{\rm C}) = \frac{\rho}{m_p}(1 + 2Y_{\rm C}). \quad (68)$$

Correspondingly, in all formulae the factor $(2 - Y_{\rm He})$ will be replaced by $(2 - Y_{\rm He} - Y_{\rm C})$, and $(8 - 5Y_{\rm He})$ by $(8 - 5Y_{\rm He} - 17Y_{\rm C}/3)$. Additionally, the right-hand side of equation (27) has to be multiplied by the factor of $(1 + 2Y_{\rm C})$. Clearly, this modification will add the fifth free parameter $Y_{\rm C}$ to the model. Using the general methodology outlined in this paper one should be able to produce solutions for the parameter p and the dilution factor. The problem that can arise from the inclusion of heavy elements is the possibility for heavy ions to be only partly ionized. The ionization degree can also vary throughout the atmosphere. Because full ionization and constancy of the gas's chemical composition are the basic assumptions of the adopted approach, we cannot explicitly include the effect of ionization in our model. Instead, it can be accounted for in a manner similar to our temperature profile correction. First, the approximate atmospheric profiles can be obtained by assuming full ionization. Then, the ionization degree can be calculated by solving the Saha equation and using this solution as a zero-order approximation of the atmospheric temperature and the electron number density profiles. Finally, one should proceed by solving the hydrodynamic problem, in which the partial ionization of heavy elements is taken into account.

For the reasons mentioned above, it is also a problem to include the proper physics for the transport of heavy nuclei to the outer layers. Two major processes can contribute to this element flow. Bulk motion mixing should dominate in the convection zone close to the bottom of the atmosphere. In the outer layers, a strong radiative push should govern the process because of the large resonance cross sections of the heavy elements. The general problem of heavy ions mixing is quite difficult and requires a rigorous approach, which is outside the scope of this paper.

As far as the boundary conditions are concerned, modeling of carbon nuclear flashes will require higher bottom temperatures. The temperature of the carbon-burning zone is argued to be about 10^{10} K (see Strohmayer & Brown 2002), which is close to the upper boundary for the bottom temperature T_b used in our calculations. No peculiarities of the approach were detected in the case of very high bottom temperatures. Extremely high temperatures will require the correct form of the opacity coefficient κ (Paczyński 1983) instead of equation (2), which represents a simplified formula for κ in the case of modest temperatures.

Another important issue is the correct accounting for the line emission of heavy elements, which is detected in the spectral analysis of superbursts. Strohmayer & Brown (2002) argued that this phenomena is caused by reflection from the accretion disk during the burst. One can estimate the disk heating time by using the standard Shakura-Sunyaev accretion-disk model (Shakura & Sunyaev 1973) and the fact that approximately 10% of the burst luminosity is absorbed by the inner part of the disk (Lapidus & Sunyaev 1985). *Simple estimates give a timescale of less than a second, assuming a mass-accretion rate of the order of Eddington or less for the disk-accretion regime, and a burst luminosity greater than 5% of Eddington, which is detected during several thousand seconds of observation of the superburst in 4U 1820−30.* Consequently, the observed spectral feature of the Kα line should be generated in the burst atmosphere rather than in the disk. The disk gains the temperature of the X-ray radiation very quickly.

Unfortunately, the origin and behavior of the spectral-line features still remain unexplained. The authors plan to include the spectral-line effect in the relaxation method in order to calculate the line emission during the X-ray burst and to compare this with the observed spectra.

Relativistic effects are usually negligible during the strong X-ray burst due to the significant radial expansion and the fact that the outgoing spectrum formation occurs at the outer layers of the atmosphere. General relativistic effects become important at the contraction stage when the extended envelope recedes close to the neutron star surface (see Lewin et al. 1993). Haberl & Titarchuk (1995) applied the full general relativity approach for a derivation of the neutron star mass-radius relation in 4U 1820−30 using *EXOSAT* observations and the T94 model.

7. CONCLUSIONS

This paper follows a common idea of the last decade to fit observational and numerical spectra with some model, mostly blackbody shapes, to obtain spectral softening/hardening factors (London et al. 1986). We improve this technique in several ways. We use more realistic non-blackbody spectral profiles for fitting, which accounts for the observed power-law soft excess of X-ray burster spectra. The temperature profile is corrected by solving the temperature equation. The existence of the isothermal photosphere during X-ray bursts is confirmed numerically and analytically. Finally, we analytically obtain the multiplicative (dilution) factor, which is not a parameter of fitting anymore, but self-consistently incorporated in the model.

We show how the theoretical study of the radiatively driven wind phenomenon can produce useful techniques for analyzing observational data. It can fulfill the needs of emerging branches of observational X-ray astronomy, such as a very promising discovery of superbursts (Strohmayer & Brown 2002) that exhibit photospheric expansion and spectral modifications relevant to extended atmospheres. We present the analytical theory of strong X-ray bursts, which includes the effects of Comptonization and free-free absorption. Partly presented in some earlier publications, this area of the study of the X-ray burst spectral formation was lacking a detailed and self-consistent account. We use numerical simulation to validate our analytical theory and to link our solution to energy axes. We show how this information can be extracted from spectral data. We provide the analytical expression for the X-ray burst spectral shape, which depends only on input physical parameters of the problem: neutron star mass, radius, surface temperature, and elemental abundance. Expressions for color ratios and dilution coefficient are also given.

The authors thank Peter Becker for valuable comments and suggestions that improved the paper. We are grateful to Menas Kafatos for encouragement and to the Center for Earth Science and Space Research (GMU) for the support of this research. We appreciate the thorough analysis of the presented work by the referee.

APPENDIX A

ANALYTIC SOLUTION FOR THE RADIATIVE TRANSFER PROBLEM

We look for the solution of equation (35) in the form

$$J(\tau, x) = \left(\frac{\tau}{\tau_{\rm th}}\right)^2 B_\nu(\tau_{\rm th}) + \tilde{J}(\tau, x) . \tag{A1}$$

The basic idea is to separate the high-frequency (diluted blackbody) and the low-frequency $\tilde{J}(\tau, x)$ parts of spectrum, where different physical processes dominate. The Kompaneets operator L_ν acting upon the blackbody shape vanishes and we neglect $L_\nu(\tilde{J})$, which allows us to get the solution of the radiative transfer problem analytically. At this point $\tau_{\rm th}$ is a parameter of the problem. The algorithm of determination of $\tau_{\rm th}$ will be described separately. Substituting equation (A1) into equation (35), we find for $\tilde{J}(\tau, x)$

$$\frac{\partial}{\partial\tau}\left(\frac{1}{\tau}\frac{\partial\tilde{J}}{\partial\tau}\right) - \frac{3}{\tau}\frac{\alpha_{\rm ff}}{\alpha_{\rm T}}\tilde{J} = -\frac{3}{\tau}\frac{\alpha_{\rm ff}}{\alpha_{\rm T}} B_\nu\left[1 - \left(\frac{\tau}{\tau_{\rm th}}\right)^2\right] , \tag{A2}$$

with a boundary condition

$$\tilde{J}_\nu|_{\tau=\tau_{\rm th}} = 0 . \tag{A3}$$

The solution satisfying this condition is presented by

$$\tilde{J}(\tau, x) = \frac{1}{pW} y_1(\tau) \int_0^{\tau_{\rm th}} y_2(\tau) f(\tau) d\tau , \tag{A4}$$

where $p(\tau) = \frac{1}{\tau}$ and $W(\tau)$ is the Wronskian:

$$W = \begin{vmatrix} y_1 & y_2 \\ y_1' & y_2' \end{vmatrix} = -\frac{7}{4}\tau . \tag{A5}$$

Thus, the product

$$pW = -\tfrac{7}{4} .$$

Functions $y_1(x)$ and $y_2(x)$ are

$$y_1(\tau) = \tau I_{4/7}\left[\tfrac{4}{7}\sqrt{3D\Psi(x)}\tau^{7/4}\right] , \tag{A6}$$

$$y_2(\tau) = \tau K_{4/7}\left[\tfrac{4}{7}\sqrt{3D\Psi(x)}\tau^{7/4}\right] , \tag{A7}$$

where $I_\nu(x)$ and $K_\nu(x)$ are modified Bessel functions of the first and the second types, respectively.

The function $f(\tau)$ in equation (A4) is the right-hand side of equation (A2), namely,

$$f(\tau) = -\frac{3}{\tau}\frac{\alpha_{\rm ff}}{\alpha_{\rm T}} = -3\tau^{1/2} D\Psi(x) B_\nu\left[1 - \left(\frac{\tau}{\tau_{\rm th}}\right)^2\right] . \tag{A8}$$

We introduce a new variable t:

$$t = \tfrac{4}{7}\sqrt{3D\Psi(x)}\tau^{7/4} , \tag{A9}$$

and rewrite equation (A4) as

$$\tilde{J}(t, x) = B_\nu t^{4/7} I_{4/7}(t) \int_0^{t_{\rm th}} t^{3/7} K_{4/7}(t)\left[1 - \left(\frac{t}{t_{\rm th}}\right)^{8/7}\right] dt . \tag{A10}$$

Using the properties of modified Bessel functions

$$\int x^p K_{p-1} dx = -x^p K_p + C , \qquad K_p = K_{-p} ,$$

we evaluate the integrals in equation (A10):

$$\int_0^{t_{\rm th}} t^{3/7} K_{4/7}(t)dt = -t^{3/7} K_{3/7}(t)\,|_0^{t_{\rm th}} = \frac{\Gamma(3/7)}{2^{4/7}} - t_{\rm th}^{3/7} K_{3/7}(t_{\rm th}) ,$$

$$\int_0^{t_{\rm th}} t^{11/7} K_{4/7}(t)dt = -t^{11/7} K_{11/7}(t)\,|_0^{t_{\rm th}} = \Gamma\left(\frac{11}{7}\right)2^{4/7} - t_{\rm th}^{11/7} K_{11/7}(t_{\rm th}) .$$

Finally $\tilde{J}(t, x)$ takes the form

$$\tilde{J}(t,\, x) = B_\nu t^{4/7} I_{4/7}(t)\left\{\frac{\Gamma(3/7)}{2^{4/7}} - \frac{\Gamma(11/7)2^{4/7}}{t_{\rm th}^{8/7}} + t_{\rm th}^{3/7}[K_{11/7}(t_{\rm th}) - K_{3/7}(t_{\rm th})]\right\}$$

$$= \tilde{J}(t, x) = B_\nu t^{4/7} I_{4/7}(t)\left[\frac{\Gamma(3/7)}{2^{4/7}} - \frac{\Gamma(11/7)2^{4/7}}{t_{\rm th}^{8/7}} + \frac{8}{7}\, t_{\rm th}^{-4/7} K_{4/7}(t_{\rm th})\right] . \tag{A11}$$

The last formula is a solution of equation (35). We can simplify this form by noting that we are interested in the solution in the outer layers of atmosphere (emergent spectrum) where $\tau \to 0$ and $t \to 0$, and we can use the asymptotic form for small arguments:

$$I_p(x) \approx \frac{1}{\Gamma(p+1)}\left(\frac{x}{2}\right)^p .$$

Making this substitution and putting the result into expression for $J(\tau, x)$ we find that second term in $\tilde{J}(\tau, x)$ cancels with the diluted blackbody term in $J(\tau, x)$, which takes the form

$$J(t, x) = B_\nu \frac{t^{8/7}}{2^{4/7}\Gamma(11/7)}\left[\frac{\Gamma(3/7)}{2^{4/7}} + \frac{8}{7}\, t_{\rm th}^{-4/7} K_{4/7}(t_{\rm th})\right] . \tag{A12}$$

APPENDIX B

SOLUTION OF THE TEMPERATURE EQUATION

Substituting relation (41) into the equation of radiative diffusion, multiplying it by x^2, and integrating over the energy range from x_* to ∞ (see T94 for definition of x_*), we get

$$\frac{1}{3}\left(\frac{d^2R}{d\tau^2} - \frac{1}{\tau}\frac{dR}{d\tau}\right)\int_{x_*}^{\infty} \frac{x^2}{e^x - 1}\, dx = [R(\tau) - 1]\int_{x_*}^{\infty} \frac{x^2}{e^x - 1}\frac{\alpha_{\rm ff}}{\alpha_{\rm T}}\, dx , \tag{B1}$$

where integrals can be approximated as

$$\int_{x_*}^{\infty} \frac{x^2}{e^x - 1} \approx \int_0^{\infty} x^2 e^{-x} dx = 2$$

and, noting that $\alpha_{\rm ff}/\alpha_{\rm T} = D\Psi(x)\tau^{3/2} \approx D\tau^{3/2}\tilde{g}(x)/x^2$, we obtain

$$\int_{x_*}^{\infty} \frac{x^2}{e^x - 1}\frac{\alpha_{\rm ff}}{\alpha_{\rm T}}\, dx \approx D\tau^{3/2}\int_{x_*}^{\infty} \frac{\tilde{g}(x)}{x}\, dx \approx \frac{1}{4}\ln^2\frac{2.25}{x_*}\, D\tau^{3/2} .$$

Here we used the fact that $\tilde{g}(x) \approx \frac{1}{2}\ln(2.35/x)$. The equation for $R(\tau)$ gets the form

$$\frac{d^2R}{d\tau^2} - \frac{1}{\tau}\frac{dR}{d\tau} = \frac{3}{8}\ln^2\frac{2.25}{x_*}\, D\tau^{3/2}[R(\tau) - 1] = \tilde{D}\tau^{3/2}[R(\tau) - 1] . \tag{B2}$$

Boundary conditions for this equation are

$$\begin{aligned} \tau \to 0 , \quad & R(\tau) \to 0 , \\ \tau \to \infty , \quad & R(\tau) \to 1 . \end{aligned} \tag{B3}$$

A general solution of equation (29) is

$$R(\tau) = 1 + \tau Z_{4/7}(\tfrac{4}{7}i\sqrt{\tilde{D}}\tau^{7/4}) , \tag{B4}$$

where $Z_{4/7}(z) = c_1 K_{4/7}(z) + c_2 I_{4/7}(z)$. In derivation of this formula we take into account a well-known theorem from ODE theory that the general solution of an inhomogeneous ODE is the sum of a general solution of the corresponding homogeneous ODE and some particular solution of the inhomogeneous ODE, which is chosen equal to unity in our case. The second boundary condition and the fact that

$$\begin{aligned} K_{4/7}(z) \to 0 , \quad & z \to \infty , \\ I_{4/7}(z) \to \infty , \quad & z \to \infty \end{aligned}$$

leave only c_1 nonzero, and the first boundary condition gives us the value for c_1, namely,

$$c_1 = -\frac{1}{\lim_{\tau \to 0} \tau K_{4/7}(4/7\sqrt{\tilde{D}}\tau^{7/4})0} = -\frac{2^{3/7}}{\Gamma(4/7)\tau_{\rm th}} ,$$

where we put $\tau_{\rm th} = (\frac{4}{7}\sqrt{\tilde{D}})^{-4/7}$. Then $R(\tau)$ reduces to

$$R(\tau) = 1 - \frac{2^{3/7}}{\Gamma(4/7)} \frac{\tau}{\tau_{\rm th}} K_{4/7}\left[\left(\frac{\tau}{\tau_{\rm th}}\right)^{7/4}\right] . \tag{B5}$$

A Taylor series expansion of $K_{4/7}$ over $\tau/\tau_{\rm th}$ yields for $R(\tau)$ the useful relation

$$R(\tau) = \frac{\Gamma(3/7)}{2^{8/7}\Gamma(11/7)} \left(\frac{\tau}{\tau_{\rm th}}\right)^2 . \tag{B6}$$

APPENDIX C

CONDITION AT THE SONIC POINT (DERIVATION OF Y_s)

We can rewrite the partial derivative in equation (18) using the obvious relation

$$\left(\frac{\partial P}{\partial \rho}\right)_\Xi = \frac{\partial P}{\partial T}\left(\frac{\partial T}{\partial \rho}\right)_\Xi + \frac{\partial P}{\partial y}\left(\frac{\partial y}{\partial \rho}\right)_\Xi .$$

Differentiating the equation of state (8) we obtain derivatives of pressure:

$$\frac{\partial P}{\partial T} = \left(1 + \frac{1}{y}\right)\frac{4aT^3}{3} , \qquad \frac{\partial P}{\partial y} = -\frac{1}{y^2}\frac{aT^4}{3} ,$$

and differentiating equation (21) with respect to ρ we get

$$\left(\frac{\partial T}{\partial \rho}\right)_\Xi = -\frac{T}{\lambda}\left(\frac{1}{y} + 4\right)\left(\frac{\partial y}{\partial \rho}\right)_\Xi .$$

On the other hand, differentiation of equation (9) gives us

$$\frac{a\mu m_p}{3k}\left(\frac{3T^2}{y}\frac{\partial T}{\partial \rho} - \frac{T^3}{y^2}\frac{\partial y}{\partial \rho}\right) = 1 .$$

Combination with the previous equation yields

$$\left(\frac{\partial y}{\partial \rho}\right)_\Xi = -\frac{3k}{a\mu m_p}\frac{y^2}{T^3}\left[\frac{\lambda}{\lambda + 3(1 + 4y)}\right] ,$$

$$\left(\frac{\partial T}{\partial \rho}\right)_\Xi = \frac{3k}{a\mu m_p T^2}\left[\frac{y(1 + 4y)}{\lambda + 3(1 + 4y)}\right] .$$

Now, combining all found derivatives we have

$$\left(\frac{\partial P}{\partial \rho}\right)_\Xi = \frac{k}{\mu m_p}\left\{4\left(1 + \frac{1}{y}\right)\left[\frac{y(1 + 4y)}{\lambda + 3(1 + 4y)}\right] + \frac{\lambda}{\lambda + 3(1 + 4y)}\right\}T$$

or, in a more compact form,

$$\left(\frac{\partial P}{\partial \rho}\right)_\Xi = \frac{k}{\mu m_p}\left[\frac{\lambda + 4(1 + y)(1 + 4y)}{\lambda + 3(1 + 4y)}\right]T , \tag{C1}$$

which is, in fact, a sonic point condition (18).

APPENDIX D

REDUCTION OF THE HYDRODYNAMICAL PROBLEM TO A FIRST-ORDER ODE

We derive an expression for the derivative of velocity v_y through v and y.

We substitute the temperature profile found in equation (21) into equation (5) to obtain ρ as a function of y:

$$\rho = \rho(y) = \frac{a\mu m_p T_b^3}{3k} y^{-3/\lambda - 1} \exp\left[-\frac{12(y - 1)}{\lambda}\right] .$$

Using this expression for $\rho(y)$ and equation (12), we get

$$r = r(v, y) = \left(\frac{\Phi}{4\pi}\right)^{1/2} \rho^{-1/2} v^{-1/2} = \left(\frac{3\Phi k}{4\pi a \mu m_p T_b^3}\right)^{1/2} y^{3/2\lambda + 1/2} \exp\left[\frac{6(y-1)}{\lambda}\right] v^{-1/2} .$$

Then we get derivatives

$$\frac{dr}{dy} = r\left[\left(\frac{3}{2\lambda} + \frac{1}{2}\right)\frac{1}{y} + \frac{6}{\lambda}\right], \qquad \frac{dr}{dv} = -\frac{r}{2v} .$$

Differentiation of equation (21) also gives us

$$\frac{dT}{dy} = T_b\, y^{-1/\lambda} \exp\left[-\frac{4(y-1)}{\lambda}\right]\left(-\frac{1}{\lambda y} - \frac{4}{\lambda}\right) = -\frac{T}{\lambda}\left(4 + \frac{1}{y}\right) .$$

By a combination of all these derivatives we obtain

$$\frac{dT}{dr} = \frac{dT}{dy}\frac{dy}{dr} = \frac{dT}{dy}\left(\frac{\partial r}{\partial y} + \frac{\partial r}{\partial v}\frac{dv}{dy}\right)^{-1} = -\frac{2T(4y+1)}{r\lambda y}\left[\left(\frac{3}{\lambda} + 1\right)\frac{1}{y} + \frac{12}{\lambda} - \frac{v'}{v}\right]^{-1} .$$

Substitution of it into equation (5) yields

$$L_r = -\frac{16\pi c k r^2 y}{\mu m_p \kappa}\frac{dT}{dr} = \frac{32\pi c k}{\mu m_p \lambda \kappa_0 (2 - Y_{\rm He})}\,\frac{(4y+1)(1+\alpha T)Tr}{[(3/\lambda + 1)1/y + 12/\lambda - v'/v]} .$$

From equation (13), however, we also have

$$L_r = \Psi - \Phi\left(h + \frac{v^2}{2} - \frac{GM_{\rm ns}}{r}\right) .$$

Equating the last two expressions for L_r we finally find v_y as

$$v_y' = f(v, y) = v\left[\left(1 + 3\,\frac{1+4y}{\lambda}\right)\frac{1}{y} - 75.2\,\frac{rT(8 - 5Y_{\rm He})(1+4y)(1+\alpha T)}{\lambda r_{b,\,6}\, T_{b,\,9}(\Psi/\Phi - v^2/2 - h + GM_{\rm ns}/r)}\right] .$$

Here $r_{b,\,6}$ and $T_{b,\,9}$ represent the neutron star radius and the bottom temperature of atmosphere in terms of 10^6 cm and 10^9 K, correspondingly.

REFERENCES

Cornelisse, R., Heise, J., Kuulkers, E., Verbunt, F., & in 't Zand, J. J. M. 2002a, A&A, in press

Cornelisse, R., Kuulkers, E., in 't Zand, J. J. M., Verbunt, F., & Heise, J. 2002b, A&A, in press

Ebisuzaki, T. 1987, PASJ, 39, 287

Ebisuzaki, T., Hanawa, T., & Sugimoto, D. 1983, PASJ, 35, 17 (EHS)

Greene, J. 1959, ApJ, 130, 693

Grindlay, J. E., & Heise, J. 1975, IAU Circ. 2879

Haberl, F., & Titarchuk, L. G. 1995, A&A, 299, 414

Kuulkers, E., Homan, J., van der Klis, M., Levin, W. H. G., & Mendez, M. 2002a, A&A, in press

Kuulkers, E., et al. 2002b, A&A, in press

Lapidus, I. I. 1991, ApJ, 377, L93

Lapidus, I. I., & Sunyaev, R. A. 1985, MNRAS, 217, 291

Lewin, W. H. G.,van Paradijs, J., & Taam, R. E. 1993, Space Sci. Rev., 62, 223

London, R. A., Taam, R. E., & Howard, H. W. 1986, ApJ, 306, 170

Nobili, L., Turolla, R., & Lapidus, I. I. 1994, ApJ, 433, 276 (NTL)

Nobili, L., Turolla, R., & Zamperi, L. 1991, ApJ, 383, 250

Paczyński, B. 1983, ApJ, 267, 315

Press, W. H., Teulkolsky, S. A., Vettering, W. T., & Flannery, B. P. 1992, Numerical Recipes (Cambridge: Cambridge Univ. Press)

Rybicki, G. B., & Lightman, A. P. 1979, Radiative Processes in Astrophysics (New York: Wiley)

Shakura, N. I., & Sunyaev, R. A. 1973, A&A, 24, 337

Strohmayer, T. E., & Brown, E. F. 2002, ApJ, 566, 1045

Thorne, K. S. 1981, MNRAS, 194, 439

Titarchukk, L. G. 1994, ApJ, 429, 340 (T94)